Case Studies in Thermal Engineering 24 (2021) 100852

Contents lists available at ScienceDirect

Case Studies in Thermal Engineering

journal homepage: http://www.elsevier.com/locate/csite

Vibration analysis of FGM plates in thermal environment resting on elastic foundation using ES-MITC3 element and prediction of ANN

Trung Thanh Tran [a], Phu-Cuong Nguyen [b,*], Quoc-Hoa Pham [c,d]

[a] Department of Mechanics, Le Quy Don Technical University, Hanoi, Vietnam
[b] Advanced Structural Engineering Laboratory, Faculty of Civil Engineering, Ho Chi Minh City Open University, Ho Chi Minh City, Vietnam
[c] Division of Computational Mathematics and Engineering, Institute for Computational Science, Ton Duc Thang University, Ho Chi Minh City, Vietnam
[d] Faculty of Civil Engineering, Ton Duc Thang University, Ho Chi Minh City, Vietnam

HIGHLIGHTS

- Extend the ES-MITC3 element for the free vibration analyses of FGM plates resting on the elastic foundation in the thermal environment.
- Investigate the influences of geometric parameters, material properties, and foundation stiffness on the free vibration of FGP plates.
- Set up an ANN to predict the fundamental frequency of FGP plates resting on the elastic foundation in the thermal environment with four input-data.

ARTICLE INFO

Keywords:
Functionally graded material (FGM)
Edge-based smoothed finite element method (ES-FEM)
Mixed interpolation of tensorial components (MITC)
Elastic foundation (EF)
Artificial neural networks (ANN)

ABSTRACT

In this article, some numerical results from the free vibration analysis of functionally graded material (FGM) plates resting on the elastic foundation (EF) in the thermal environment are presented. An ES-FEM combining with the MITC3 is used to improve the accuracy as well as eliminate the shear locking phenomena for the classical triangular element. The EF is modeled from the Winkler-Pasternak foundation with stiffness two-parameter. Numerical examples are compared with published works to prove the reliability and accuracy of the proposed method. The effects of volume fraction index (n), temperature (T), and two-parameter of the EF on the free vibration of FGM plates are also investigated. Furthermore, an artificial neural network (ANN) is trained to predict exactly the fundamental frequency of FGM plates.

1. Introduction

The structures on the elastic foundation (EF) are usually used in civil engineering as aircraft runways, building foundation slabs, railway tracks, and so on. In the published articles, the Winkler foundation (one-parameter) [1] or Winkler-Pasternak foundation (two-parameter) [2] are priority applied. Some typical works of the free vibration analysis of isotropic plate structures on the EF can be found in Refs. [3–6]. With the plates made by the FG material lying on the EF, Ferreira et al. [7] employed radial basis functions to examine the bending and free vibration of the FG porous plates. Shahsavari et al. [8] based on a new quasi-3D theory to investigate the

* Corresponding author.
E-mail addresses: cuong.pn@ou.edu.vn, henycuong@gmail.com (P.-C. Nguyen), phamquochoa@tdtu.edu.vn (Q.-H. Pham).

https://doi.org/10.1016/j.csite.2021.100852
Received 3 October 2020; Received in revised form 31 December 2020; Accepted 15 January 2021
Available online 23 January 2021

free vibration of FGM plates. Baferani and his co-workers [9] used the third-order shear deformation theory (TSDT) to analyze the free vibration of the FGM rectangular plate on the EF. Besides, Zenkour and Radwan [10] developed a four-unknown plate theory to study the free vibration response for the composite and sandwich plates. Duc et al. [11] employed an analytical method (AM) to analyze the nonlinear thermal dynamic behavior of FGM plates. In Ref. [12], he also studied the static bending and free vibration of FG carbon nanotube-reinforced composite plates using the AM. Mahmoudi et al. [13] based on a refined quasi-3D to investigate the FG sandwich plates on the EF subjected to thermo-mechanical loading. Thang et al. [14] calculated the buckling of FGM variable-thickness plates on the EF under compressive loading. Thien et al. [15] analyzed the buckling of nanoplates on the EF using isogeometric analysis (IGA). Thanh et al. [16] employed an ES-FEM to study the dynamic response of FGP plates and sandwich auxetic honeycomb plates on the EF [17] under moving loads. Ke et al. [18,19] used FEM to investigate the static bending, vibration, and buckling response of FG nanoplates lying on the EF.

Recently, the mechanical behavior of FGM structures subjected to different loads in the high-temperature environment is studied by many researchers. For example, Talha et al. [20] used the TSDT to consider the static and dynamic responses of FGM plates with different boundary conditions (BC). Zenkour [21] and Shen et al. [22] computed the deflection, bending moments, and stresses of the FGM plate on the EF under uniform and sinusoidal loads in a thermal environment. Moreover, the buckling analyses of FG plates under the thermal loads have also been widely discussed in Refs. [23–31]. Nuttawit et al. [32] analyzed the dynamic response of FGM plates under high temperature by using an improved TSDT. Tinh et al. [33] examined the mechanical behavior of FGM plates at high temperatures using TSDT combine with FEM, and in Ref. [34], Shen analyzed nonlinear FGM plates/shells under mechanical and thermal loads.

In the efforts to enhance the performance of the structural analysis, the MITC3 element [35] has combined with the ES-FEM [36] to create the ES-MITC3 element [37–43]. Using the ES-MITC3 element, the stiffness matrix is calculated over the edges of the MITC3 elements instead of over the element as the classical FEM. The numerical results showed that the ES-MITC3 has many superior properties in the mechanic problem such as [37]: (1) it can avoid transverse shear locking even the thickness of the structure is very minimum; (2) it has better accuracy than the original triangular elements and MITC3 [35], DSG3 [44] and CS-DSG3 [45]; and is a good competitor with the MITC4 element [46] which set the same number of nodes. In the latest researches, to enhance the efficiency of FEM for analyzing the mechanical behavior of structures, Shuhui Ren and co-workers proposed a stabilized node-based smoothed radial point interpolation method (SNS-RPIM) to investigate the behavior of functionally graded magneto-electro-elastic (FGMEE) structures in the thermal environment [47] and in the hydrothermal environment [48]. Zhou et al. [49] analyzed the dynamic response of intelligent composite structures under the thermal and mechanical loads using the cell-based smoothed finite element method (CS-FEM) and the coupled multi-physics CS-FEM (so-call CPCS-FEM). They point out that their method is higher accuracy, lower mesh restriction, and much less calculation than the classical FEM. Zhou and his colleagues [50] also employed the CS-FEM to analyze time-dependent mechanical responses of MEE structures around Curie temperature. In addition, readers can find valuable results on the mechanical behavior of MEE structures in Refs. [51–53].

Nowadays, the applying of artificial intelligence (AI) in science as well as in mechanical problems becomes a hot trend. ANN is one of the types of AI that works based on the flexible, simultaneous working process of the human brain and imitates how the human brain works. The ANN can be processed with numerous data at the same time with less cost of time. In detail, after the training process, the neural network can be perceived as the similarities from the new input data [54]. Some publications used AI to present mechanical behaviors such as the design of experiments [55], genetic algorithms [56], optimization [57], fuzzy logic [58], and finite element analysis [59], and so on. Esmailzadeh et al. [60] combined FEM with an ANN to simulate an equal channel angular pressing for the process of creating an aluminum alloy. Miguel et al. [61] created an ANN to predict exactly the buckling load of the beam subjected to uniformly loads. The ANN models can predict the fundamental frequencies of structures with input data large enough. Furthermore, using the ANN model helps reduce computation time and cost.

Based on the above-mentioned article review, the purpose of this paper now is to extend the ES-MITC3 element for the free vibration analyses of FGM plates resting on the EF in the thermal environment and create an ANN to predict the fundamental frequency of them. The numerical results compare with other published researches to verify the effectiveness of our work. Finally, the influences

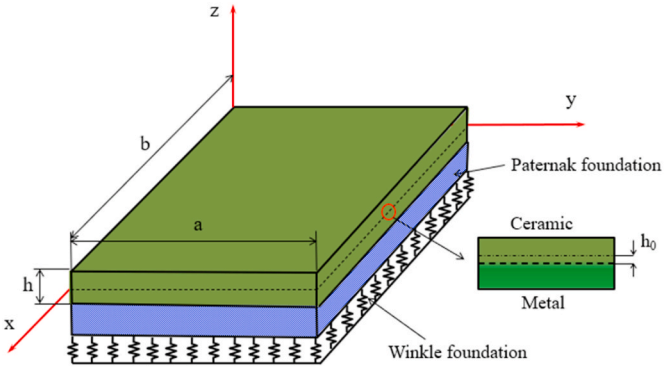

Fig. 1. The FGM plate is resting on EF.

of geometric parameters, material properties on the free vibration of FGP plates are also studied.

2. Modeling the FGM plate resting on EF

Fig. 1 displays the FGM plate on the EF. The distance between the physical neutral surface and the geometric middle surface is determined as follows [34]:

$$h_0 = \int_{-h/2}^{h/2} zE(z)dz \Big/ \int_{-h/2}^{h/2} E(z)dz \tag{1}$$

The volume ratio of ceramics and metals varies through thickness following formulation [34]:

$$V_c + V_m = 1 \;\; and \;\; V_c(z) = \left(\frac{z}{h} + \frac{1}{2}\right)^n \tag{2}$$

with $-h/2 \le z \le h/2$, n is the volume fraction index. Subscripts c and m represent the ceramic and metal components, respectively. The properties of FGM change through thickness with the volume fraction index (n) and temperature (T) expressed as [33]:

$$P(T,z) = (P_c(T) - P_m(T))V_c + P_m(T) \tag{3}$$

where: P is a symbol for Young's modulus (E); Poisson' ratio (ν); mass density of material (ρ) and coefficient of thermal expansion (α).

Material properties of ceramic and metal vary in temperature as follows [33]:

$$P(T) = P_0\left(P_{-1}T^{-1} + 1 + P_1T + P_2T^2 + P_3T^3\right) \tag{4}$$

with P_0, P_{-1} P_1 P_2, P_3 depend on different materials.

The temperature varies through thickness of the FGM plate is written by Ref. [33]:

$$T(z) = T_m + (T_c - T_m)\Lambda(z) \tag{5}$$

in which T_c, T_m are respectively the temperature of ceramic and metal. The temperature distribution function $\Lambda(z)$ is given by Ref. [33]:

$$\Lambda(z) = \frac{1}{C}\left[\left(\frac{1}{2} + \frac{z+h_0}{h}\right) - \frac{K_{cm}}{(n+1)K_m}\left(\frac{1}{2} + \frac{z+h_0}{h}\right)^{n+1} + \frac{K_{cm}^2}{(2n+1)K_{cm}^2}\left(\frac{1}{2} + \frac{z+h_0}{h}\right)^{2n+1} - \frac{K_{cm}^3}{(3n+1)K_{cm}^3}\left(\frac{1}{2} + \frac{z+h_0}{h}\right)^{3n+1} + \frac{K_{cm}^4}{(4n+1)K_{cm}^4}\left(\frac{1}{2} + \frac{z+h_0}{h}\right)^{4n+1} - \frac{K_{cm}^5}{(5n+1)K_{cm}^5}\left(\frac{1}{2} + \frac{z+h_0}{h}\right)^{5n+1}\right] \tag{6}$$

in which

$$C = 1 - \frac{K_{cm}}{(n+1)K_m} + \frac{K_{cm}^2}{(2n+1)K_{cm}^2} - \frac{K_{cm}^3}{(3n+1)K_{cm}^3} + \frac{K_{cm}^4}{(4n+1)K_{cm}^4} - \frac{K_{cm}^5}{(5n+1)K_{cm}^5}$$
$$K_{cm} = K_c - K_m \tag{7}$$

with K_c, K_m are respectively thermal conductivity of ceramic and metal.

In this work, the EF is Winkler-Pasternak foundation model [2] with two parameters, the relationship between force and displacement in this foundation is modeled as follows:

$$\mathbf{q}_e = k_1 w(x,y) - k_2\left(\frac{\partial^2}{\partial x^2} + \frac{\partial^2}{\partial y^2}\right)w(x,y) \tag{8}$$

with w is the displacement along z-axis; k_1 and k_2 are respectively two-parameter of foundation stiffness. The Winkler-Pasternak foundation also includes the Winkler foundation when ignoring the effect of shear parameter (k_2).

3. The first-order shear deformation theory and weak form of FGM plates

3.1. First-order shear deformation theory for FGM plates

The displacement field of the FGM plate based on the FSDT as follows [62]:

$$\begin{cases} u(x,y,z) = u_0(x,y) + (z-h_0)\theta_x(x,y) \\ v(x,y,z) = v_0(x,y) + (z-h_0)\theta_y(x,y) \\ w(x,y,z) = w_0(x,y) \end{cases} \tag{9}$$

in which u_0, v_0, w_0, θ_x, θ_y are five unknown displacements of the mid-surface of plates. The strain field can be written by:

$$\boldsymbol{\varepsilon} = \boldsymbol{\varepsilon_m} + (z - h_0)\boldsymbol{\kappa} \tag{10}$$

The membrane strain

$$\boldsymbol{\varepsilon_m} = \begin{Bmatrix} u_{0,x} \\ v_{0,y} \\ u_{0,y} + v_{0,x} \end{Bmatrix} \tag{11}$$

The bending and transverse shear strains

$$\boldsymbol{\kappa} = \begin{Bmatrix} \theta_{x,x} \\ \theta_{y,y} \\ \theta_{x,y} + \theta_{y,x} \end{Bmatrix} \tag{12}$$

$$\boldsymbol{\gamma} = \begin{Bmatrix} w_{0,x} + \theta_x \\ w_{0,y} + \theta_y \end{Bmatrix} \tag{13}$$

The stress-strain relations of the plate can be obtained as

$$\begin{Bmatrix} \sigma_x \\ \sigma_y \\ \tau_{xy} \\ \tau_{xz} \\ \tau_{yz} \end{Bmatrix} = \begin{bmatrix} Q_{11} & Q_{12} & 0 & 0 & 0 \\ Q_{21} & Q_{22} & 0 & 0 & 0 \\ 0 & 0 & Q_{66} & 0 & 0 \\ 0 & 0 & 0 & Q_{55} & 0 \\ 0 & 0 & 0 & 0 & Q_{44} \end{bmatrix} \begin{Bmatrix} \varepsilon_x \\ \varepsilon_y \\ \gamma_{xy} \\ \gamma_{xz} \\ \gamma_{yz} \end{Bmatrix} \tag{14}$$

in which

$$\begin{aligned} &Q_{11} = Q_{22} = \frac{E(T,z)}{1-\nu(T,z)^2}; Q_{12} = Q_{21} = \frac{\nu(T,z)E(T,z)}{1-\nu(T,z)^2}; \\ &Q_{44} = Q_{55} = Q_{66} = \frac{E(T,z)}{2(1+\upsilon(T,z))} \end{aligned} \tag{15}$$

3.2. Weak form equations

Using Hamilton's principle, we obtain the motion equations of the plate as follows [62]:

$$\int_{t_1}^{t_2} (\delta\mathscr{U} - \delta\mathscr{K})\mathrm{d}t = 0 \tag{16}$$

where the strain energy $\mathscr{U}$ is defined as

$$\mathscr{U} = \mathscr{U}^p + \mathscr{U}^f \tag{17}$$

with $\mathscr{U}^f$ represents the strain energy of the foundation:

$$\mathscr{U}^f = \frac{1}{2}\int_{\psi} \left(k_1 w^2 - k_2 \left[\left(\frac{\partial^2 w}{\partial x^2} \right)^2 + \left(\frac{\partial^2 w}{\partial y^2} \right)^2 \right] \right) \mathrm{d}\psi \tag{18}$$

and $\mathscr{U}^p$ is the strain energy of plates:

$$\mathscr{U}^p = \frac{1}{2}\int_{\psi} \left(\boldsymbol{\varepsilon}^T \boldsymbol{D}_b \boldsymbol{\varepsilon} + \boldsymbol{\gamma}^T \boldsymbol{D}_s \boldsymbol{\gamma} \right) \mathrm{d}\psi \tag{19}$$

in which $\boldsymbol{\varepsilon} = [\boldsymbol{\varepsilon_m} \quad \boldsymbol{\kappa}]^T$ and

$$\boldsymbol{D}_b = \begin{bmatrix} \boldsymbol{A} & \boldsymbol{B} \\ \boldsymbol{B} & \boldsymbol{F} \end{bmatrix} \tag{20}$$

$\boldsymbol{A}$ $\boldsymbol{B}$, $\boldsymbol{F}$, and $\boldsymbol{D}_s$ are determined by

$$(\boldsymbol{A}, \boldsymbol{B}, \boldsymbol{F}) = \int_{-h/2}^{h/2} \left(1, (z-h_0), (z-h_0)^2\right) \begin{bmatrix} Q_{11} & Q_{12} & 0 \\ Q_{21} & Q_{22} & 0 \\ 0 & 0 & Q_{66} \end{bmatrix} \mathrm{d}z \tag{21}$$

$$\boldsymbol{D}_s = \int_{-h/2}^{h/2} \begin{bmatrix} Q_{55} & 0 \\ 0 & Q_{44} \end{bmatrix} dz \tag{22}$$

The kinetic energy of the plate

$$\mathscr{K} = \frac{1}{2} \int_{\Psi} \dot{\boldsymbol{u}}^T \boldsymbol{m} \dot{\boldsymbol{u}} d\Psi \tag{23}$$

in which $\boldsymbol{u}^T = \begin{bmatrix} u_0 & v_0 & w_0 & \theta_x & \theta_y \end{bmatrix}$, and $\boldsymbol{m}$ is obtained by:

$$\mathbf{m} = \begin{bmatrix} I_1 & 0 & 0 & I_2 & 0 \\ & I_1 & 0 & 0 & I_2 \\ & & I_1 & 0 & 0 \\ & & & I_3 & 0 \\ & & & & I_3 \end{bmatrix} \tag{24}$$

in there $(I_1, I_2, I_3) = \int_{-h/2}^{h/2} \rho(1, (z - h_0), (z - h_0)^2) \mathrm{d}z$.

Substituting Eqs. 17 and 23 into Eq. (16), we obtain the weak form formulation following as

$$\int_{\psi} \delta \boldsymbol{\varepsilon}^T \boldsymbol{D}_b \boldsymbol{\varepsilon} \mathrm{d} + \int_{\psi} \delta \boldsymbol{\gamma}^T \boldsymbol{D}_s \boldsymbol{\gamma} \mathrm{d}\psi + \int_{\psi} \delta \boldsymbol{w}^T \left[k_1 \boldsymbol{w} - k_2 \left(\frac{\partial^2 \boldsymbol{w}}{\partial x^2} + \frac{\partial^2 \boldsymbol{w}}{\partial y^2} \right) \right] d\Psi = \int_{\Psi} \dot{\boldsymbol{u}}^T \mathbf{m} \dot{\boldsymbol{u}} d\Psi \tag{25}$$

4. An ES-MITC3 method for the plate

4.1. Formulation of the MITC3 element

The bounded domain of plates $\psi \subset \mathscr{R}^2$ is disjointed into n^e finite triangular elements with n^n nodes such that $\psi \approx \sum_{e=1}^{n^e} \psi_e$ and $\psi_i \cap \psi_j = \varnothing,\ i \neq j$. When the displacements $\boldsymbol{u}^e = [u_j^e,\ v_j^e,\ w_j^e,\ \theta_{xj}^e,\ \theta_{yj}^e]^T$ of element ψ_e are approached as [35]:

$$\boldsymbol{u}^e(\boldsymbol{x}) = \sum_{j=1}^{n^{ne}} \begin{bmatrix} N_I(\mathrm{x}) & 0 & 0 & 0 & 0 \\ 0 & N_I(\mathrm{x}) & 0 & 0 & 0 \\ 0 & 0 & N_I(\mathrm{x}) & 0 & 0 \\ 0 & 0 & 0 & N_I(\mathrm{x}) & 0 \\ 0 & 0 & 0 & 0 & N_I(\mathrm{x}) \end{bmatrix} \boldsymbol{d}_j^e = \sum_{j=1}^{n^{ne}} \boldsymbol{N}(\mathbf{x}) \boldsymbol{d}_j^e \tag{26}$$

where n^{ne} is the total of nodes; $\boldsymbol{N}(\mathbf{x})$ presents the shape function; and $\boldsymbol{d}_j^e = [u_j^e,\ v_j^e,\ w_j^e, \theta_{xj}^e,\ \theta_{yj}^e]^T$ are the degrees of freedom (DOF) of a node.

The strain field of MITC3 element is indicated as follows:

$$\boldsymbol{\varepsilon}_m^e = [\boldsymbol{B}_{m1}^e \quad \boldsymbol{B}_{m2}^e \quad \boldsymbol{B}_{m3}^e] \boldsymbol{d}^e = \boldsymbol{B}_m^e \boldsymbol{d}^e \tag{27}$$

$$\boldsymbol{\kappa}^e = [\boldsymbol{B}_{b1}^e \quad \boldsymbol{B}_{b2}^e \quad \boldsymbol{B}_{b3}^e] \boldsymbol{d}^e = \boldsymbol{B}_b^e \boldsymbol{d}^e \tag{28}$$

where

$$\boldsymbol{B}_{m1}^e = \frac{1}{2A_e} \begin{bmatrix} b-c & 0 & 0 & 0 & 0 \\ 0 & d-a & 0 & 0 & 0 \\ d-a & b-c & 0 & 0 & 0 \end{bmatrix}, \tag{29}$$

$$\boldsymbol{B}_{m2}^e = \frac{1}{2A_e} \begin{bmatrix} c & 0 & 0 & 0 & 0 \\ 0 & -d & 0 & 0 & 0 \\ -d & c & 0 & 0 & 0 \end{bmatrix}, \tag{30}$$

$$\boldsymbol{B}_{m3}^e = \frac{1}{2A_e} \begin{bmatrix} -b & 0 & 0 & 0 & 0 \\ 0 & a & 0 & 0 & 0 \\ a & -b & 0 & 0 & 0 \end{bmatrix}, \tag{31}$$

$$\boldsymbol{B}_{b1}^e = \frac{1}{2A_e} \begin{bmatrix} 0 & 0 & 0 & b-c & 0 \\ 0 & 0 & 0 & 0 & d-a \\ 0 & 0 & 0 & d-a & b-c \end{bmatrix}, \tag{32}$$

$$\boldsymbol{B}_{b2}^{e}=\frac{1}{2A_e}\begin{bmatrix}0&0&0&c&0\\0&0&0&0&-d\\0&0&0&-d&c\end{bmatrix}, \tag{33}$$

$$\boldsymbol{B}_{b3}^{e}=\frac{1}{2A_e}\begin{bmatrix}0&0&0&-b&0\\0&0&0&0&a\\0&0&0&a&-b\end{bmatrix}, \tag{34}$$

The formulation of the MITC3 element based on FSDT [35] to avoid shear locking problem is represented as follows:

$$\boldsymbol{\gamma}^{e}=\boldsymbol{B}_{s}^{e}\boldsymbol{d}^{e} \tag{35}$$

in which

$$\boldsymbol{B}_{s}^{e}=[\boldsymbol{B}_{s1}^{e}\quad\boldsymbol{B}_{s2}^{e}\quad\boldsymbol{B}_{s3}^{e}] \tag{36}$$

with

$$\boldsymbol{B}_{s1}^{e}=\boldsymbol{J}^{-1}\begin{bmatrix}0&0&-1&\frac{a}{3}+\frac{d}{6}&\frac{b}{3}+\frac{c}{6}\\0&0&-1&\frac{d}{3}+\frac{a}{6}&\frac{c}{3}+\frac{b}{6}\end{bmatrix} \tag{37}$$

$$\boldsymbol{B}_{s2}^{e}=\boldsymbol{J}^{-1}\begin{bmatrix}0&0&1&\frac{a}{2}-\frac{d}{6}&\frac{b}{2}-\frac{c}{6}\\0&0&0&\frac{d}{6}&\frac{c}{6}\end{bmatrix} \tag{38}$$

$$\boldsymbol{B}_{s3}^{e(0)}=\boldsymbol{J}^{-1}\begin{bmatrix}0&0&0&\frac{a}{6}&\frac{b}{6}\\0&0&1&\frac{d}{2}-\frac{a}{6}&\frac{c}{2}-\frac{b}{6}\end{bmatrix} \tag{39}$$

where

$$\boldsymbol{J}^{-1}=\frac{1}{2A_e}\begin{bmatrix}c&-b\\-d&a\end{bmatrix} \tag{40}$$

in which $a=x_2-x_1$, $b=y_2-y_1$, $c=y_3-y_1$, $d=x_3-x_1$, and A_e is the area of the triangular element as indicated in Fig. 2. Substituting the displacement field into Eq. (25), the system equation for the free vibration analysis of plates is expressed as follows:

$$(\boldsymbol{K}-\omega^2\boldsymbol{M})\boldsymbol{d}=0 \tag{41}$$

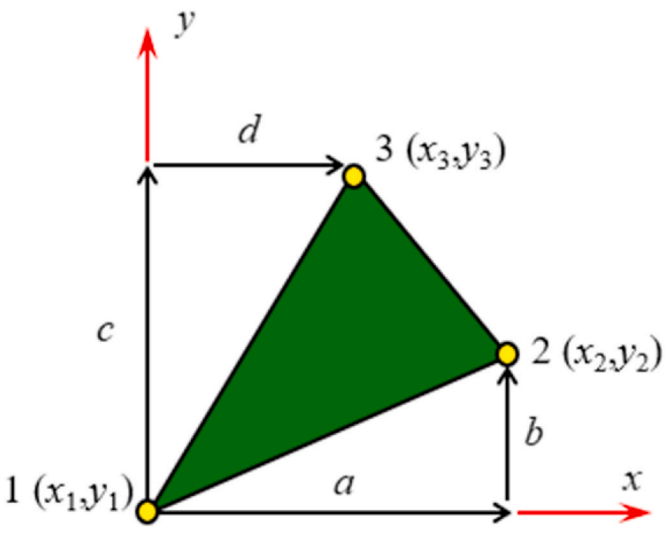

Fig. 2. Model of the triangular element.

where $\boldsymbol{K}$ and $\boldsymbol{M}$ are the stiffness and mass matrices.

The stiffness matrix:

$$\boldsymbol{K} = \sum_{e=1}^{n^e} \left(\boldsymbol{K}_p^e + \boldsymbol{K}_f^e \right), \tag{42}$$

where

$$\boldsymbol{K}_p^e = \int_{\Psi_e} \boldsymbol{B}^T \boldsymbol{D}_b \boldsymbol{B} \mathrm{d}\psi_e + \int_{\Psi_e} \boldsymbol{B}_s^T \boldsymbol{D}_s \boldsymbol{B}_s \mathrm{d}\psi_e \tag{43}$$

and

$$\boldsymbol{K}_f^e = k_1 \int_{\Psi_e} \mathbf{N}_w^{\mathrm{T}} \mathbf{N}_w \mathrm{d}\psi_e + \mathrm{k}_2 \int_{\Psi_e} \left[\left(\frac{\partial \mathbf{N}_w}{\partial \mathrm{x}} \right)^{\mathrm{T}} \left(\frac{\partial \mathbf{N}_w}{\partial \mathrm{x}} \right) + \left(\frac{\partial \mathbf{N}_w}{\partial \mathrm{y}} \right)^{\mathrm{T}} \left(\frac{\partial \mathbf{N}_w}{\partial \mathrm{y}} \right) \right] \mathrm{d}\psi_e \tag{44}$$

in which

$$\boldsymbol{B}^e = [\, \boldsymbol{B}_m^e \quad \boldsymbol{B}_b^e \,] \tag{45}$$

$$\mathbf{N}_w = [00N_1 00, 00N_2 00, 00N_3 00] \tag{46}$$

The mass matrix:

$$\boldsymbol{M} = \sum_{e=1}^{n^e} \boldsymbol{M}_p^e \tag{47}$$

where

$$\boldsymbol{M}_p^e = \int_{\Psi_e} \boldsymbol{N}^T \boldsymbol{m} \boldsymbol{N} \mathrm{d}\psi_e \tag{48}$$

4.2. An ES-MITC3 method for FGP plates

The smoothing domains ψ^k is built based on edges of the MITC3 elements such that $\psi = \cup_{k=1}^{n^k} \psi^k$ and $\psi_i^k \cap \psi_j^k = \varnothing$ for $i \neq j$. An edge-based smoothing domain ψ^k connected with the inner edge k is formed by connecting two end-nodes of the edge to the centroids of adjacent triangular elements, as depicted in Fig. 3.

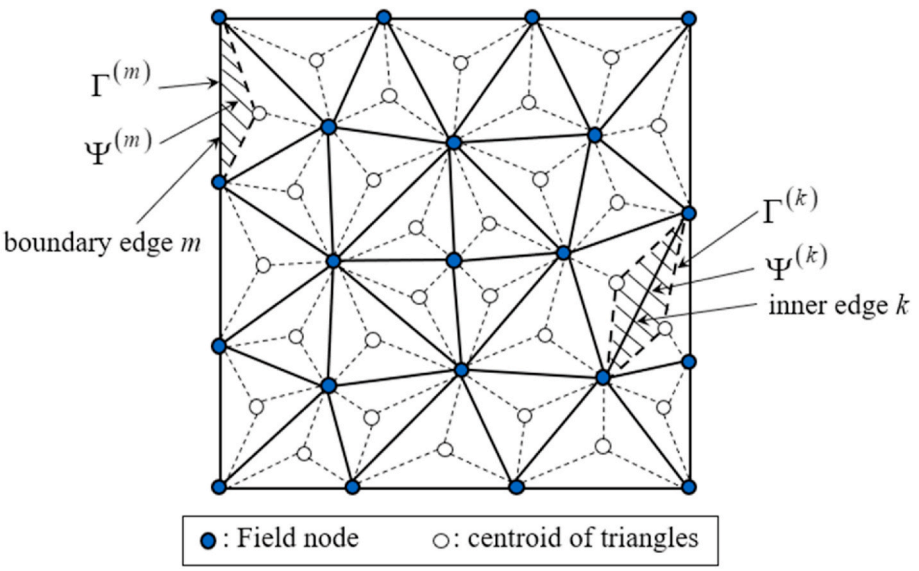

Fig. 3. The smoothing domain ψ^k of triangular elements.

Using the edge-based smooth technique [37], the strain fields $\widetilde{\boldsymbol{\varepsilon}}_m^k$, $\widetilde{\boldsymbol{\kappa}}^k$, $\widetilde{\boldsymbol{\gamma}}^k$ over the smoothing domain ψ^k are calculated as:

$$\widetilde{\boldsymbol{\varepsilon}}_m^k = \int_{\psi^k} \boldsymbol{\varepsilon}_m \, \Phi^k(\mathbf{x}) \mathrm{d}\psi, \tag{49}$$

$$\widetilde{\boldsymbol{\kappa}}^k = \int_{\psi^k} \boldsymbol{\kappa} \, \Phi^k(\mathbf{x}) \mathrm{d}\psi, \tag{50}$$

$$\widetilde{\boldsymbol{\gamma}}^k = \int_{\psi^k} \boldsymbol{\gamma} \, \Phi^k(\mathbf{x}) \mathrm{d}\psi, \tag{51}$$

where $\Phi^k(\mathbf{x})$ is a smoothing function that satisfies at least $\int_{\psi^k} \Phi^k(\mathbf{x}) \mathrm{d}\psi = 1$.

Using the constant smoothing function as [37]:

$$\Phi^k(\mathbf{x}) = \begin{cases} \dfrac{1}{A^k} & x \in \psi^k \\ 0 & x \notin \psi^k \end{cases} \tag{52}$$

in which A^k is the area of domain ψ^k with:

$$A^k = \int_{\psi^k} \mathrm{d}\psi = \frac{1}{3} \sum_{i=1}^{n^{ek}} A^i \tag{53}$$

where n^{ek} is the total MITC3 elements in the smoothing domain ψ^k; and A^i is the area of the ith element attached to the edge. k.

Substituting Eqs. (49)–(51) into Eqs. (27), (28) and (35), the strain field of the smoothing domain ψ^k can be defined by:

$$\widetilde{\boldsymbol{\varepsilon}}_m^k = \sum_{j=1}^{n^{nk}} \widetilde{\mathbf{B}}_{mj}^k \boldsymbol{d}_j^k; \;\; \widetilde{\boldsymbol{\kappa}}^k = \sum_{j=1}^{n_{sh}^{nk}} \widetilde{\mathbf{B}}_{bj}^k \boldsymbol{d}_j^k; \;\; \widetilde{\boldsymbol{\gamma}}^k = \sum_{j=1}^{n_{sh}^{nk}} \widetilde{\mathbf{B}}_{sj}^k \boldsymbol{d}_j^k; \tag{54}$$

where n_{sh}^{nk} is the total of nodes of the MITC3 elements attached to edge k ($n_p^{nk} = 1$ for boundary edges and $n_p^{nk} = 2$ for inner edges as given in Fig. 3; $\boldsymbol{d}_j^k$ is the DOFs of nodes connected with the smoothing domain ψ^k; $\widetilde{\mathbf{B}}_{mj}^k$, $\widetilde{\mathbf{B}}_{bj}^k$, and $\widetilde{\mathbf{B}}_{sj}^k$ computed by

$$\widetilde{\mathbf{B}}_{mj}^k = \frac{1}{A^k} \sum_{i=1}^{n^{ek}} \frac{1}{3} A^i \boldsymbol{B}_{mj}^e \tag{55}$$

$$\widetilde{\boldsymbol{B}}_{bj}^k = \frac{1}{A^k} \sum_{i=1}^{n^{ek}} \frac{1}{3} A^i \boldsymbol{B}_{bj}^e \tag{56}$$

$$\widetilde{\boldsymbol{B}}_{sj}^k = \frac{1}{A^k} \sum_{i=1}^{n^{ek}} \frac{1}{3} A^i \boldsymbol{B}_{sj}^e \tag{57}$$

Then, the stiffness matrix of the FGM plate is assembled by

$$\widetilde{\mathbf{K}} = \sum_{k=1}^{n_{sh}^k} \widetilde{\mathbf{K}}^k \tag{58}$$

where $\widetilde{\mathbf{K}}^k$ is the ES-MITC3 stiffness and computed by

$$\widetilde{\boldsymbol{K}}^k = \int_{\psi^k} \left(\widetilde{\boldsymbol{B}}^{kT} \boldsymbol{D}_b \widetilde{\boldsymbol{B}}^k + \widetilde{\boldsymbol{B}}_s^{kT} \boldsymbol{D}_b \widetilde{\boldsymbol{B}}_s^k \right) d\psi = \widetilde{\boldsymbol{B}}^{kT} \boldsymbol{D}_b \widetilde{\boldsymbol{B}}^k A^k + \widetilde{\boldsymbol{B}}_s^{kT} \boldsymbol{D}_s \widetilde{\boldsymbol{B}}_s^k A^k \tag{59}$$

in which

$$\widetilde{\boldsymbol{B}}^{kT} = \begin{bmatrix} \widetilde{\boldsymbol{B}}_{mj}^k & \widetilde{\boldsymbol{B}}_{bj}^k \end{bmatrix} \tag{60}$$

5. Accuracy of the ES-MITC3 element

Firstly, authors consider the fully simple support (SSSS) FGM plate (Al/Al_2O_3) with their material properties: metal (Al) $E_m = 70$ GPa, $\rho_m = 2702\ kg/m^3$, and ceramic (Al_2O_3) $E_c = 380$ GPa, $\rho_c = 3800\ kg/m^3$, $\upsilon = 0.3$ are fixed. The following non-dimensional parameters are defined by Refs. [8,9]:

$$K_1 = \frac{k_1 a^4}{H_m}; K_2 = \frac{k_2 a^2}{H_m} with\ H_m = \frac{E_m h^3}{12(1-\upsilon^2)};\ \Omega = \omega h\sqrt{\frac{\rho_m}{E_m}} \tag{61}$$

It can be found that the numerical results of the present method agree well with those by an analytical method based on a new quasi-3D hyperbolic theory [8], more accurate than using TSDT [9] and the original MITC3 element as shown in Table 1.

Secondly, the non-dimensional fundamental frequencies of a fully clamped (CCCC) FGM plate in thermal environments (without the EF) are studied. The material properties are shown in Table 2, the volume fraction index is $n = 1$. The geometrical parameters of the plate are considered: $b = a$; $h/a = 0.1$. The non-dimensional fundamental frequency is determined by the formulation:

$$\Omega = \omega \frac{b^2}{h}\sqrt{\rho_0 \frac{(1-\nu_0^2)}{E_0}} \tag{61}$$

where E_0 and ρ_0 are the reference values of E_m and ρ_m at $T_0 = 300K$.

The numerical results of the proposed method are compared with those in the literature [32,33] and presented in Table 3. These results agree well with those in published work [33] which use FEM based on the TSDT, and the error is about 3.5% when compared with reported results using the analytical method [32]. It means that the present method is highly reliable.

6. Numerical results

In this subsection, an SSSS FGM plate in a thermal environment with $T_c = 400K$ and $T_m = 300K$. The geometrical parameters $a = b$, $h = a/50$ and the stiffness of EF: $K_1 = 100$, $K_2 = 10$ are considered. The material properties are listed in Table 2 with the volume fraction index $n = 1$. The first six non-dimensional fundamental frequencies of the FGM plate are listed in Table 4. Besides, the first six mode shapes are also plotted in Fig. 4. The foundation stiffness and non-dimensional fundamental frequencies as follow Eq. (62) with $H_0 = \frac{E_0 h^3}{12(1-\nu_0^2)}$; in which E_0, ρ_0, and ν_0 are the reference values of E_m, ρ_m, and ν_m at $T_0 = 300K$, respectively. It can be seen that the second and third mode shapes are similar to each other (the fundamental frequencies are approximated to each other, the difference is due to the direction of the observation). It is suitable for the symmetrical plates under the same boundary conditions.

6.1. Effect of temperature T and volume fraction index n

To examine the effects of temperature and volume fraction index, we now examine the SSSS FGM plate with $a = b$, $h = a/25$. The material properties of FGM are listed in Table 2. Temperature value T_c change from 300 to 1500K, $T_m = 300K$ is fixed. The volume fraction index gets values. $n = 0, 1, 2, 5, 10, \infty$.

From Fig. 5 and Table 5, it can be seen that when the increase of T_c and n gives the non-dimensional fundamental frequencies of plate decrease. It is understandable because T_c and n increase leads to the stiffness of the plate decreases while the mass of the plate does not change. Specifically, when the increase of n from 0 to 10 gives the first non-dimensional fundamental frequency of the plate decreases strongly, and it changes very little when n is greater than 10. It also can be seen that when T_c changes from 300 K to 1000 K leads to the slight change of the first non-dimensional fundamental frequency of the plate and the decrease of the first non-dimensional fundamental frequency of the plate when T_c is bigger 1000 K. In all of the cases, the ceramic-rich plates have greater hardness and better heat resistance than the metal plates. High strength and good heat resistance are the basic properties of structures made of the

Table 1
The first non-dimensional fundamental frequencies of FGM plates according to the EF.

(K_1, K_2)	k	Present	Δ(%)	MITC3	Δ(%)	[9]	Δ(%)	[8]
(0, 0)	0	0.0291	0.000	0.0291	0.000	0.0290	0.344	0.0291
	1	0.0225	0.442	0.0225	0.442	0.0227	0.442	0.0226
	2	0.0205	0.485	0.0205	0.485	0.0209	1.456	0.0206
	5	0.0194	0.513	0.0194	0.513	0.0197	1.026	0.0195
(100, 0)	0	0.0298	0.000	0.0301	1.007	0.0298	0.000	0.0298
	1	0.0235	0.424	0.0235	0.424	0.0238	0.847	0.0236
	2	0.0217	0.459	0.0216	0.917	0.0221	1.376	0.0218
	5	0.0207	0.481	0.0207	0.481	0.0210	0.962	0.0208
(100, 100)	0	0.0411	0.000	0.0413	0.487	0.0411	0.000	0.0411
	1	0.0385	0.259	0.0385	0.259	0.0388	0.518	0.0386
	2	0.0381	0.522	0.0381	0.522	0.0386	0.783	0.0383
	5	0.0384	0.260	0.0384	0.260	0.0388	0.779	0.0385

Table 2
Temperature-dependent coefficients of FGM plates.

Material	Properties	P_0	P_{-1}	P_1	P_2	P_3
Si_3N_4	E_c (Pa)	349.43×10^9	0	-3.070×10^{-4}	2.160×10^{-7}	-8.946×10^{-11}
	α_c (1/K)	5.8723×10^{-6}	0	9.095×10^{-4}	0	0
	K_c (W/m K)	13.72	0	0	0	0
	ν_c	0.240	0	0	0	0
	ρ_c (kg/m^3)	2370	0	0	0	0
$SU304$	E_m (Pa)	201.04×10^9	0	3.079×10^{-4}	$-653{,}4 \times 10^{-7}$	0
	α_m (1/K)	12.330×10^{-6}	0	8.086×10^{-4}	0	0
	K_m (W/m K)	15.379	0	0	0	0
	ν_m	0.326	0	-2.002×10^{-4}	3.797×10^{-7}	0
	ρ_m (kg/m^3)	8166	0	0	0	0

Table 3
Non-dimensional fundamental frequencies of FGM plates in thermal environments.

	$\Delta T = 100\ K$	$\Delta T = 200\ K$	$\Delta T = 300\ K$
Present	13.4393	13.2936	13.1163
Δ(%)	3.41	1.25	1.35
MITC3	13.3821	13.2371	13.0606
Δ(%)	3.82	1.67	0.92
[33]	13.433	13.280	13.093
Δ(%)	3.46	1.35	1.17
[32]	13.915	13.462	12.941

Note that: $\Delta(\%) = 100 \times \frac{|\Omega_{pre} - \Omega_{fre}|}{\Omega_{fre}}$ with Ω_{pre} is the non-dimensional fundamental frequency in this paper and Ω_{fre} is non-dimensional fundamental frequencies in references.

Table 4
Non-dimensional fundamental frequencies of the FGM plate.

Ω_1	Ω_2	Ω_3	Ω_4	Ω_5	Ω_6
0.0808	0.1936	0.1941	0.299	0.3655	0.3655

FG materials.

6.2. Effect of the stiffness of the EF

Next, the influences of the foundation stiffness K_1, K_2 are investigated. Let us consider a SSSS FGM plate has $a = b,\ h = a/\ 25;\ K_1$ change from 10 to 100, K_2 from 0 to 10, and the volume fraction index is $n = 1$. The first non-dimensional fundamental frequency of the FGM plate is presented in Table 6 and shown in Fig. 6. From these figures and tables, it can be observed that the increase of K_1 and K_2 gives the non-dimensional fundamental frequency increases. This problem can be explained that two parameters of foundation make the plate stiffness greater, and when the increase of temperature leads to the plate stiffness reduces. We also can be found that the stiffness of Pasternak K_2 is more effective than the stiffness of Winkler K_1.

6.3. Creating an ANN model

To predict the non-dimensional fundamental frequencies of the plate, we first have to train the ANN model by several sets of material parameters, stiffness of EF, and non-dimensional fundamental frequencies. We set up the ANN model to have four input data: temperature (T_c), volume fraction index (n), stiffness of the foundation K_1, K_2; one data output is the non-dimensional fundamental frequencies (see Fig. 7). In this model, we randomly choose fifteen data input for training in a total of 20, and the rest five data to test. In this work, the ANN is designed in MATLAB software. It contains the following 3 layers: Input layer - the activity of the input data represents the raw information that can feed into the network, Hidden layer - to determine the activity of each hidden data. The activities of the input data and the weights on the associations of the input and the hidden data. There may have one or more hidden layers and the output layer. The output data depends on the activity of the hidden data and the weights between the hidden and output data. To prepare for this work, three files are created: *Data_input, Data_output*, and *Predict_output*. In which *Data_input* includes material

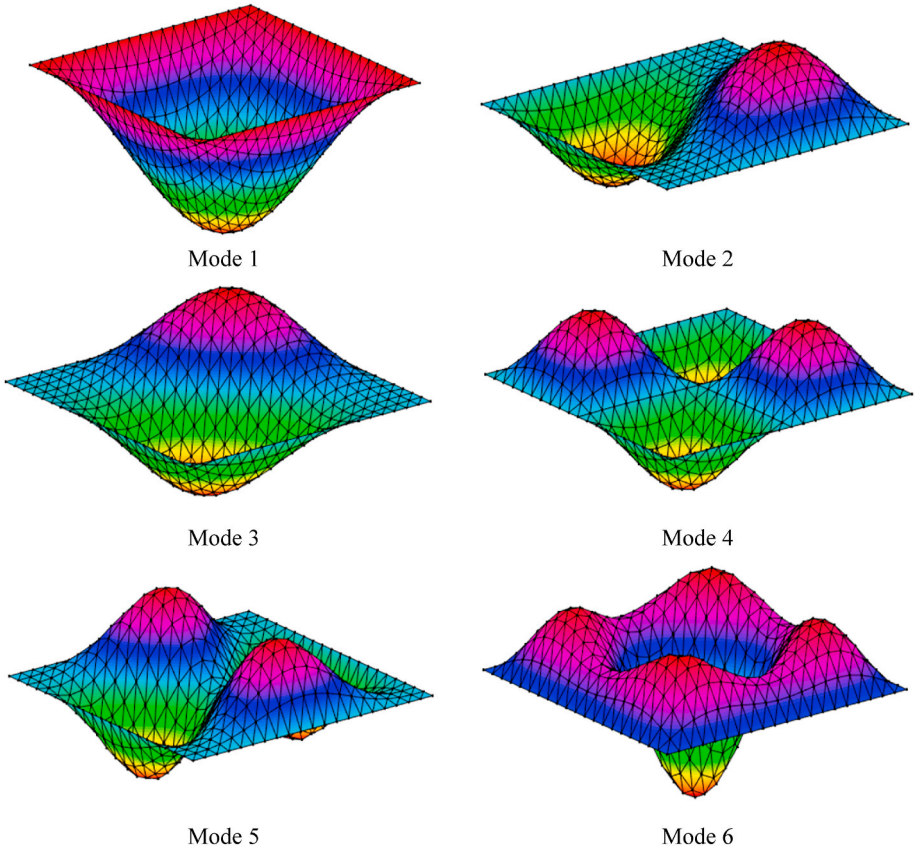

Fig. 4. The six mode shapes the FGM plate resting on EF in thermal environments.

parameters and stiffness of foundation, *Data_output* is the first non-dimensional fundamental frequencies of the FGM plate (these frequencies are calculated in the previous section), and *Predict_output* includes material parameters and the foundation stiffness of the ANN to predict the first non-dimensional fundamental frequencies. Then, by using the established calculation program, the authors calculated the first non-dimensional fundamental frequencies separately and compared them with ANN's predicted results. In a hidden layer, we change the number of neurons from 5 to 20. The training time of an ANN depends strongly on weight and bias updates. In MATLAB software, the weights are automatically updated after each value of the input data. Furthermore, there is one-parameter as the momentum value is used to avoid stuck in local optimization. Besides, the learning rate is often established the data in a range of 0.001–10. It depends on during the training process, and the momentum has remained at an average value equal to 0.8. After the training process, we find that twenty neurons achieved the most accurate prediction of frequencies. Results of training are presented in Table 7. The predicted result of non-dimensional fundamental frequencies by the ANN is listed in Table 8. The percentage error is defined as follows:

$$\Delta(\%) = 100 \times \frac{|Predict\ data - Computation\ data|}{computation\ data} \tag{62}$$

From Table 8, it can be seen that errors are less than 2%. This ANN algorithm can predict exactly the non-dimensional fundamental frequencies of the FGM plate. Thus, the model can be applied to different structures, which only need to set the input data, detail targets, the number of input data, testing, and choose the number of neurons of the hidden layers also as the momentum.

7. Conclusions

In this article, the free vibration of FGM plates on the EF in the thermal environment is investigated. We used the ES-MITC3 element to create the governing equation of FGM plates. An ANN is also created to predict the non-dimensional fundamental frequencies. Our work has the following advantages:

Using the ES-MITC3 element represents a good agreement with the other methods. It is also more accurate than using the classical MITC3 and original triangular element.

Set up an ANN model that can be predicted relatively accurate non-dimensional fundamental frequencies of FGM plate with input four-parameter.

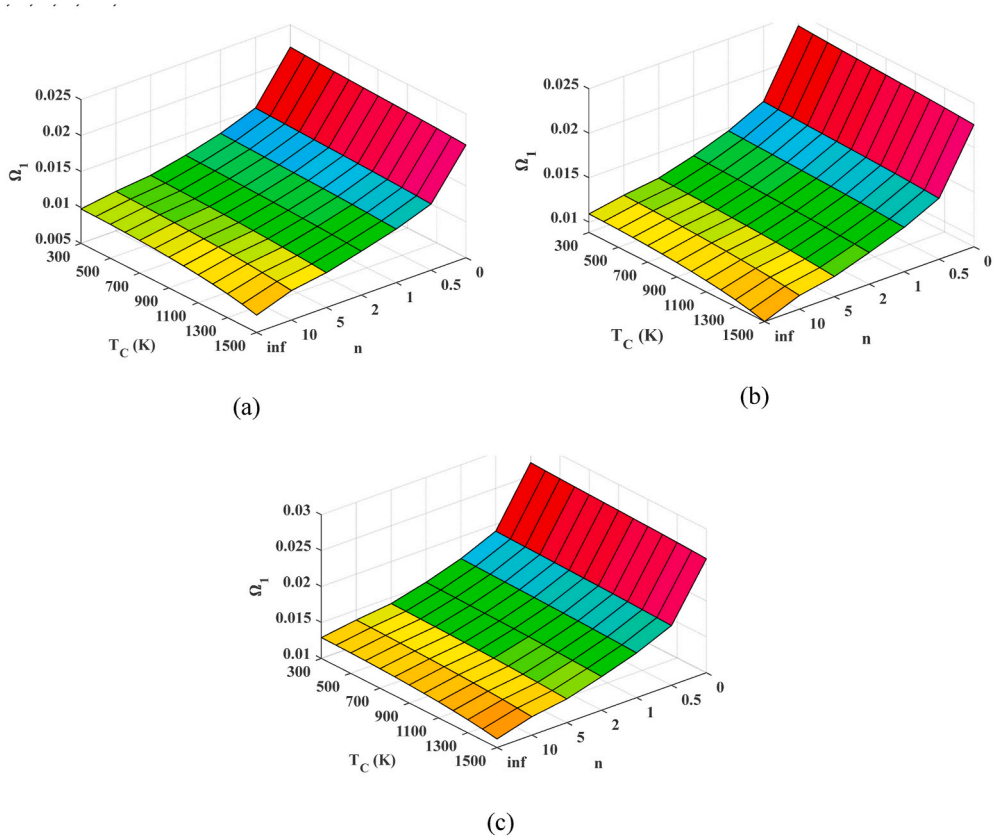

Fig. 5. The first non-dimensional fundamental frequencies of the FGM plate with various values of T and n. (a) $K_1 = K_2 = 0$; (b) $K_1 = 100$; $K_2 = 0$; (c) $K_1 = 100$; $K_2 = 10$.

Table 5
The first non-dimensional fundamental frequencies of the FGM plate on the EF.

$(K_1; K_2)$	T_c	n					
		0	1	2	5	10	∞
(0; 0)	300	0.02190	0.01517	0.01337	0.01206	0.01100	0.01051
	500	0.02168	0.01502	0.01325	0.01195	0.01090	0.01041
	700	0.02149	0.01489	0.01313	0.01184	0.01079	0.01028
	900	0.02132	0.01476	0.01300	0.01171	0.01064	0.01011
	1100	0.02114	0.01461	0.01285	0.01155	0.01044	0.00987
	1300	0.02094	0.01444	0.01268	0.01135	0.01019	0.00954
	1500	0.02070	0.01422	0.01245	0.01110	0.00986	0.00910
(100; 0)	300	0.02367	0.01657	0.01467	0.01327	0.01215	0.01164
	500	0.02347	0.01643	0.01455	0.01317	0.01206	0.01156
	700	0.02330	0.01631	0.01444	0.01307	0.01196	0.01144
	900	0.02314	0.01619	0.01433	0.01295	0.01182	0.01128
	1100	0.02297	0.01606	0.01420	0.01281	0.01165	0.01107
	1300	0.02279	0.01590	0.01404	0.01264	0.01142	0.01078
	1500	0.02256	0.01570	0.01383	0.01241	0.01113	0.01039
(100; 10)	300	0.02684	0.01904	0.01695	0.01540	0.01417	0.01362
	500	0.02667	0.01893	0.01685	0.01532	0.01409	0.01355
	700	0.02652	0.01882	0.01676	0.01523	0.01400	0.01345
	900	0.02638	0.01871	0.01666	0.01513	0.01388	0.01331
	1100	0.02623	0.01860	0.01654	0.01501	0.01374	0.01313
	1300	0.02607	0.01846	0.01641	0.01486	0.01355	0.01289
	1500	0.02587	0.01830	0.01623	0.01467	0.01330	0.01256

Table 6
Non-dimensional fundamental frequencies of the FGM plate with various values of K_1 and K_2.

Temperature	K_2	K_1				
		10	30	50	70	100
$T_c = 300\,K$ $T_m =$ $300\,K$	0	0.01351	0.01377	0.01404	0.01429	0.01467
	3.0	0.01429	0.01454	0.01479	0.01503	0.01539
	5.0	0.01478	0.01503	0.01527	0.01550	0.01585
	7.0	0.01526	0.01550	0.01573	0.01596	0.01630
	10	0.01596	0.01618	0.01641	0.01663	0.01695
$T_c = 1000\,K$ $T_m = 300\,K$	0	0.01307	0.01335	0.01361	0.01388	0.01427
	3.0	0.01387	0.01413	0.01439	0.01464	0.01501
	5.0	0.01438	0.01463	0.01488	0.01512	0.01548
	7.0	0.01488	0.01512	0.01536	0.01559	0.01594
	10	0.01559	0.01582	0.01605	0.01627	0.01660
$T_c = 1500\,K$ $T_m = 300\,K$	0	0.01260	0.01288	0.01316	0.01343	0.01383
	3.0	0.01343	0.01370	0.01396	0.01422	0.01460
	5.0	0.01396	0.01421	0.01447	0.01472	0.01508
	7.0	0.01446	0.01471	0.01496	0.01520	0.01555
	10	0.01519	0.01543	0.01566	0.01589	0.01623

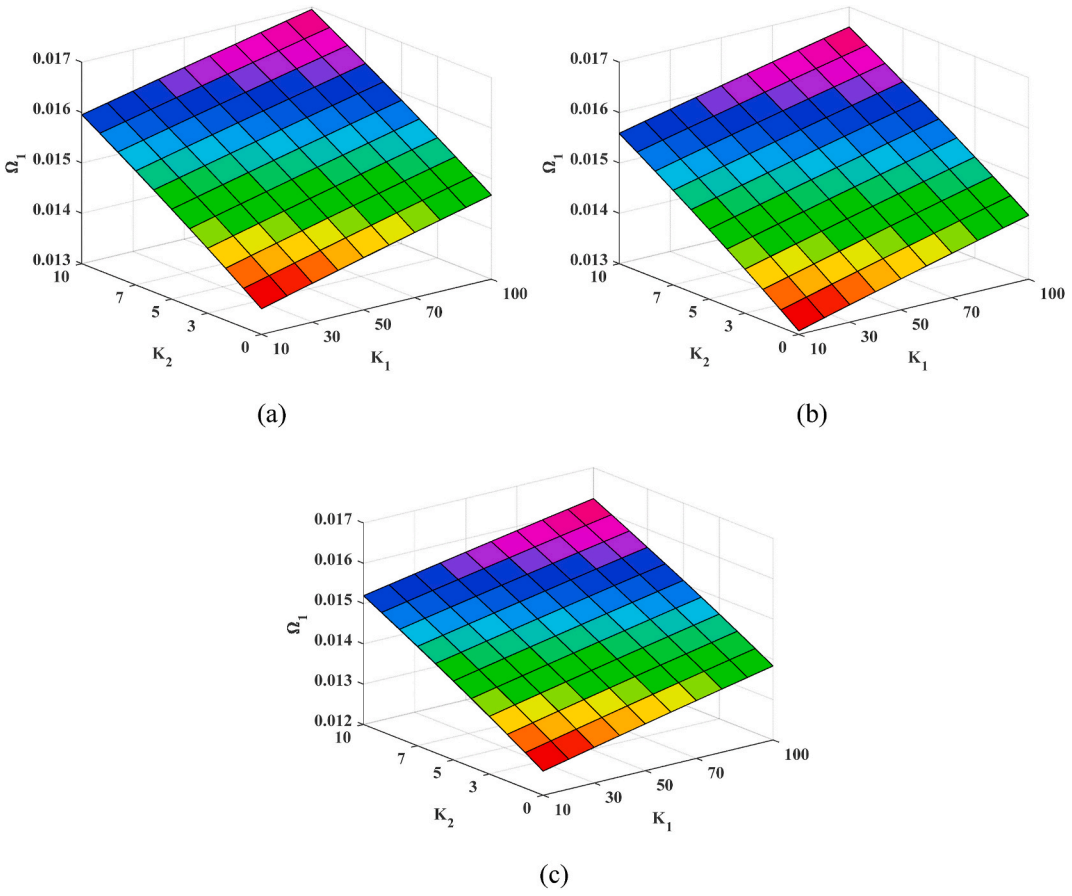

Fig. 6. Non-dimensional fundamental frequencies of the FGM plate with various values K_1, K_2.
(*a*) $T_c = T_m = 300\,K$; (b) $T_c = 1000\,K$; $T_m = 300\,K$; (c) $T_c = 1500\,K$; $T_m = 300\,K$.

Two parameters of the EF are K_1 and K_2 increase stiffness, while the increase of temperature decrease stiffness of the FGM plate.

The material parameter n also influences on the free vibration of the plates. Specifically, increasing n leads to the stiffness of the plate decreases due to the volume factor of ceramic in the plate reduces.

This study can expand to analyze other structures resting on the EF in the thermal environment using different theories. Set up an ANN in Matlab software to predict output-parameter for complicated mechanical systems.

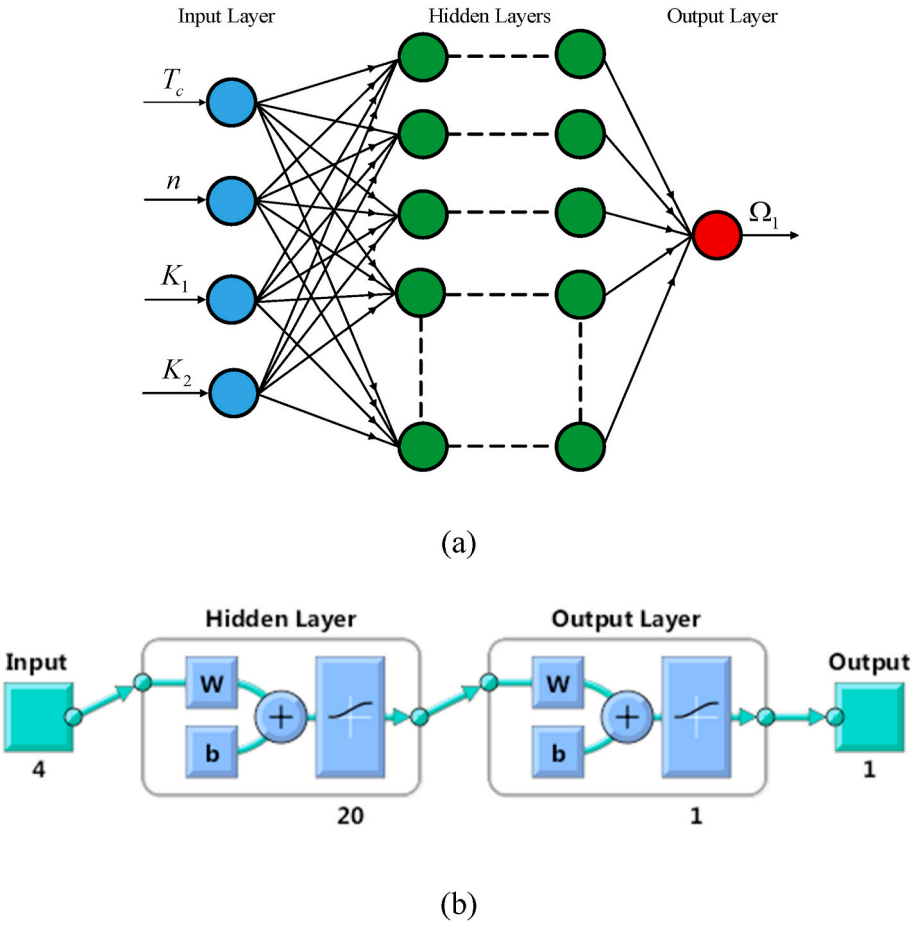

Fig. 7. The ANN with four input data and one output data. (a) Flowchart of the ANN with four input data; (b) Modeling the ANN in Matlab software.

Table 7
The input and output data of the ANN for the training process.

Order	T_c (K)	n	K_1	K_2	Target (Ω_1)	Prediction (Ω_1)	Δ (%)
1	300	1	10	0	0.01351	0.01351	0.00
2	500	1	100	0	0.01643	0.01643	0.00
3	500	5	100	0	0.01317	0.01317	0.00
4	500	10	100	0	0.01206	0.01206	0.00
5	1000	1	50	5	0.01488	0.01488	0.00
6	1000	1	100	5	0.01548	0.01548	0.00
7	1500	0	100	10	0.02587	0.02587	0.00
8	1500	2	100	10	0.01623	0.01623	0.00
9	1500	5	100	10	0.01467	0.01467	0.00
10	1500	10	100	10	0.01330	0.01330	0.00
11	1000	1	10	3	0.01387	0.01387	0.00
12	1000	1	30	3	0.01413	0.01413	0.00
13	1000	1	50	3	0.01439	0.01439	0.00
14	1000	1	70	3	0.01464	0.01464	0.00
15	1000	1	100	3	0.01501	0.01501	0.00

Author agreement statement

We the undersigned declare that this manuscript is original, has not been published before and is not currently being considered for publication elsewhere. We confirm that the manuscript has been read and approved by all named authors and that there are no other persons who satisfied the criteria for authorship but are not listed. We further confirm that the order of authors listed in the manuscript has been approved by all of us. We understand that the Corresponding Author is the sole contact for the Editorial process. He/she is

Table 8
Input data and numerical results are predicted by this ANN model.

Order	T_c (K)	n	K_1	K_2	Computation (Ω_1)	Prediction (Ω_1)	Δ (%)
1	500	2	100	0	0.01455	0.01465	0.69
2	1000	1	10	5	0.01438	0.01437	0.07
3	1000	1	30	5	0.01463	0.01442	1.44
4	1000	1	70	5	0.01512	0.01536	1.59
5	1500	1	100	10	0.01830	0.01829	0.05

responsible for communicating with the other authors about progress, submissions of revisions and final approval of proofs.

Declaration of competing interest

There is no conflict of interest.

References

[1] E. Winkler, Die Lehre von der Elasticitaet und Festigkeit, in: E. Winkler (Ed.), Dominicus, 1867.
[2] P.L. Pasternak, On a New Method of Analysis of an Elastic Foundation Using Two Foundation Constants, Gosudarstvennoe Izdatelstvo Literaturi po Stroitelstvu i Arkhitekture, 1954, pp. 1–56.
[3] A.W. Leissa, The free vibration of plates, J. Sound Vib. 31 (1973) 257–293, https://doi.org/10.1016/S0022-460X(73)80371-2.
[4] Y. Xiang, C.M. Wang, S. Kitipornchai, Exact vibration solution for initially stressed Mindlin plates on Pasternak foundation, Int. J. Mech. Sci. 36 (1994) 311–316, https://doi.org/10.1016/0020-7403(94)90037-X.
[5] M.H. Omurtag, A. Ozutok, A.Y. Akoz, Free vibration analysis of Kirchhoff plates resting on the elastic foundation by mixed finite element formulation based on gateaux differential, Int. J. Numer. Methods Eng. 40 (1997) 295–317, https://doi.org/10.1002/(SICI)1097-0207(19970130)40:2<295::AID-NME66>3.0.CO;2-2.
[6] D. Zhou, Y.K. Cheung, S.H. Lo, F.T.K. Au, Three-dimensional vibration analysis of rectangular thick plates on pasternak foundation, Int. J. Numer. Methods Eng. 59 (2004) 1313–1334, https://doi.org/10.1002/nme.915.
[7] A.J.M. Ferreira, C.M.C. Roque, A.M.A. Neves, R.M.N. Jorge, C.M.M. Soares, Analysis of plates on Pasternak foundations by radial basis functions, Comput. Mech. 46 (2010) 791–803, https://doi.org/10.1007/s00466-010-0518-9.
[8] D. Shahsavari, M. Shahsavari, L. Li, B. Karami, A novel quasi-3D hyperbolic theory for free vibration of FG plates with porosities resting on Winkler/Pasternak/Kerr foundation, Aero. Sci. Technol. 72 (2018) 134–149, https://doi.org/10.1016/j.ast.2017.11.004.
[9] A. Hasani Baferani, A.R. Saidi, H. Ehteshami, Accurate solution for free vibration analysis of functionally graded thick rectangular plates resting on elastic foundation, Compos. Struct. 93 (2011) 1842–1853, https://doi.org/10.1016/j.compstruct.2011.01.020.
[10] A.M. Zenkour, A.F. Radwan, Free vibration analysis of multilayered composite and softcore sandwich plates resting on Winkler-Pasternak foundations, J. Sandw. Struct. Mater. 20 (2018) 169–190, https://doi.org/10.1177/1099636216644863.
[11] N.D. Duc, D.H. Bich, P.H. Cong, Nonlinear thermal dynamic response of shear deformable FGM plates on elastic foundations, J. Therm. Stresses 39 (2016) 278–297, https://doi.org/10.1080/01495739.2015.1125194.
[12] N.D. Duc, J. Lee, T. Nguyen-Thoi, P.T. Thang, Static response and free vibration of functionally graded carbon nanotube-reinforced composite rectangular plates resting on Winkler-Pasternak elastic foundations, Aero. Sci. Technol. 68 (2017) 391–402, https://doi.org/10.1016/j.ast.2017.05.032.
[13] A. Mahmoudi, S. Benyoucef, A. Tounsi, A. Benachour, E.A. Adda Bedia, S.R. Mahmoud, A refined quasi-3D shear deformation theory for thermo-mechanical behaviour of functionally graded sandwich plates on elastic foundations, J. Sandw. Struct. Mater. 21 (2019) 1906–1929, https://doi.org/10.1177/1099636217727577.
[14] P.-T. Thang, T. Nguyen-Thoi, J. Lee, Closed-form expression for nonlinear analysis of imperfect sigmoid-FGM plates with variable thickness resting on elastic medium, Compos. Struct. 143 (2016) 143–150, https://doi.org/10.1016/j.compstruct.2016.02.002.
[15] T. Banh-Thien, H. Dang-Trung, L. Le-Anh, V. Ho-Huu, T. Nguyen-Thoi, Buckling analysis of non-uniform thickness nanoplates in an elastic medium using the Isogeometric analysis, Compos. Struct. 162 (2017) 182–193, https://doi.org/10.1016/j.compstruct.2016.11.092.
[16] T.T. Tran, Q.-H. Pham, T. Nguyen-Thoi, Dynamic analysis of functionally graded porous plates resting on elastic foundation taking into mass subjected to moving loads using an edge-based smoothed finite element method, Shock Vib. 2020 (2020) 1–19, https://doi.org/10.1155/2020/8853920.
[17] T.T. Tran, Q.-H. Pham, T. Nguyen-Thoi, T.-V. Tran, Dynamic analysis of sandwich auxetic honeycomb plates subjected to moving oscillator load on elastic foundation, Advances in Materials Science and Engineering 2020 (2020) 1–16, https://doi.org/10.1155/2020/6309130.
[18] V.-K. Tran, T.-T. Tran, M.-V. Phung, Q.-H. Pham, T. Nguyen-Thoi, A finite element formulation and nonlocal theory for the static and free vibration analysis of the sandwich functionally graded nanoplates resting on elastic foundation, J. Nanomater. 2020 (2020), https://doi.org/10.1155/2020/8786373.
[19] V.-K. Tran, Q.-H. Pham, T. Nguyen-Thoi, A finite element formulation using four-unknown incorporating nonlocal theory for bending and free vibration analysis of functionally graded nanoplates resting on elastic medium foundations, Eng. Comput. (2020) 1–26, https://doi.org/10.1007/s00366-020-01107-7.
[20] M. Talha, B.N. Singh, Static response and free vibration analysis of FGM plates using higher-order shear deformation theory, Appl. Math. Model. 34 (2010) 3991–4011, https://doi.org/10.1016/j.apm.2010.03.034.
[21] A.M. Zenkour, The refined sinusoidal theory for FGM plates on elastic foundations, Int. J. Mech. Sci. 51 (2009) 869–880, https://doi.org/10.1016/j.ijmecsci.2009.09.026.
[22] H.-S. Shen, Z.-X. Wang, Nonlinear bending of FGM plates subjected to combined loading and resting on elastic foundations, Compos. Struct. 92 (2010) 2517–2524, https://doi.org/10.1016/j.compstruct.2010.02.010.
[23] E. Feldman, J. Aboudi, Buckling analysis of functionally graded plates subjected to uniaxial loading, Compos. Struct. 38 (1997) 29–36, https://doi.org/10.1016/S0263-8223(97)00038-X.
[24] W. Lanhe, Thermal buckling of a simply supported moderately thick rectangular FGM plate, Compos. Struct. 64 (2004) 211–218, https://doi.org/10.1016/j.compstruct.2003.08.004.
[25] R. Javaheri, M.R. Eslami, Thermal buckling of functionally graded plates based on higher-order theory, J. Therm. Stresses 25 (2002) 603–625, https://doi.org/10.1080/01495730290074333.
[26] X. Zhao, Y.Y. Lee, K.M. Liew, Mechanical and thermal buckling analysis of functionally graded plates, Compos. Struct. 90 (2009) 161–171, https://doi.org/10.1016/j.compstruct.2009.03.005.
[27] B.A.S. Shariat, M.R. Eslami, Thermal buckling of imperfect functionally graded plates, Int. J. Solid Struct. 43 (2006) 4082–4096, https://doi.org/10.1016/j.ijsolstr.2005.04.005.
[28] H.M. Navazi, H. Haddadpour, Nonlinear cylindrical bending analysis of shear deformable functionally graded plates under different loading using analytical methods, Int. J. Mech. Sci. 50 (2008) 1650–1657, https://doi.org/10.1016/j.ijmecsci.2008.08.010.

[29] Y. Kiani, E. Bagherizadeh, M.R. Eslami, Thermal buckling of clamped thin rectangular FGM plates resting on Pasternak elastic foundation (Three approximate analytical solutions), J. Appl. Math. Mech. 91 (2011) 581–593, https://doi.org/10.1002/zamm.201000184.

[30] J.-S. Park, J.-H. Kim, Thermal post-buckling and vibration analyses of functionally graded plates, J. Sound Vib. 289 (2006) 77–93, https://doi.org/10.1016/j.jsv.2005.01.031.

[31] H.-S. Shen, Thermal post-buckling behaviour of shear deformable FGM plates with temperature-dependent properties, Int. J. Mech. Sci. 49 (2007) 466–478, https://doi.org/10.1016/j.ijmecsci.2006.09.011.

[32] N. Wattanasakulpong, G.B. Prusty, D.W. Kelly, Free and forced vibration analysis using improved third-order shear loading deformation theory for functionally graded plates under high temperature, J. Sandw. Struct. Mater. 15 (2013), https://doi.org/10.1177/1099636213495751.

[33] T.Q. Bui, T.V. Do, L.H.T. Ton, D.H. Doan, S. Tanaka, D.T. Pham, T.-A. Nguyen-Van, T. Yu, S. Hiros, On the high-temperature mechanical behaviours analysis of heated functionally graded plates using FEM and a new third-order shear deformation plate theory, Compos. B Eng. 92 (2016) 218–241, https://doi.org/10.1016/j.compositesb.2016.02.048.

[34] H.-S. Shen, in: H.-S. Shen (Ed.), Functionally Graded Materials: Nonlinear Analysis of Plates and Shell, CRC Press, 2009, https://doi.org/10.1201/9781420092578.

[35] P.-S. Lee, K.-J. Bathe, Development of MITC isotropic triangular shell finite elements, Comput. Struct. 82 (2004) 945–962, https://doi.org/10.1016/j.compstruc.2004.02.004.

[36] G. Liu, T. Nguyen-Thoi, K. Lam, An edge-based smoothed finite element method (ES-FEM) for static, free and forced vibration analyses of solids, J. Sound Vib. 320 (2009) 1100–1130, https://doi.org/10.1016/j.jsv.2008.08.027.

[37] T. Chau-Dinh, Q. Nguyen-Duy, H. Nguyen-Xuan, Improvement on MITC3 plate finite element using edge-based strain smoothing enhancement for plate analysis, Acta Mech. 228 (2017) 2141–2163, https://doi.org/10.1007/s00707-017-1818-3.

[38] T.-K. Nguyen, V.-H. Nguyen, T. Chau-Dinh, T.P. Vo, H. Nguyen-Xuan, Static and vibration analysis of isotropic and functionally graded sandwich plates using edge-based MITC3 finite elements, Compos. B Eng. 107 (2016) 162–173, https://doi.org/10.1016/j.compositesb.2016.09.058.

[39] Q.-H. Pham, T.-V. Tran, T.-D. Pham, D.-H. Phan, An edge-based smoothed MITC3 (ES-MITC3) shell finite element in laminated composite shell structures analysis, Int. J. Comput. Methods 15 (2017) 1850060, https://doi.org/10.1142/S0219876218500603.

[40] Q.-H. Pham, T.-D. Pham, Q.V. Trinh, D.-H. Phan, Geometrically nonlinear analysis of functionally graded shells using an edge-based smoothed MITC3 (ES-MITC3) finite elements, Eng. Comput. 36 (2020) 1069–1082, https://doi.org/10.1007/s00366-019-00750-z.

[41] D. Pham-Tien, H. Pham-Quoc, T. Vu-Khac, N. Nguyen-Van, Transient analysis of laminated composite shells using an edge-based smoothed finite element method, International Conference on Advances in Computational Mechanics (2017) 1075–1094, https://doi.org/10.1007/978-981-10-7149-2_75.

[42] T.T. Tran, Q.H. Pham, T. Nguyen-Thoi, Static and Free Vibration Analyses of Functionally Graded Porous Variable Thickness Plates Using an Edge-Based Smoothed Finite Element Method, Defence Technology, 2020, https://doi.org/10.1016/j.dt.2020.06.001.

[43] T.T. Tran, Q.H. Pham, T. Nguyen-Thoi, An edge-based smoothed finite element for free vibration analysis of functionally graded porous (FGP) plates on elastic foundation taking into mass (EFTIM), Math. Probl Eng. 2020 (2020) 1–17.

[44] K.-U. Bletzinger, M. Bischoff, E. Ramm, A unified approach for shear-locking-free triangular and rectangular shell finite elements, Comput. Struct. 75 (2000) 321–334, https://doi.org/10.1016/S0045-7949(99)00140-6.

[45] T. Nguyen-Thoi, P. Phung-Van, H. Nguyen-Xuan, C. Thai-Hoang, A cell-based smoothed discrete shear gap method (CS-DSG3) using triangular elements for static and free vibration analyses of Reissner-Mindlin plates, Int. J. Numer. Methods Eng. 91 (2012) 705–741, https://doi.org/10.1002/nme.4289.

[46] K.-J. Bathe, E.N. Dvorkin, A formulation of general shell elements-the use of mixed interpolation of tensorial components, Int. J. Numer. Methods Eng. 22 (1986) 697–722, https://doi.org/10.1002/nme.1620220312.

[47] S. Ren, G. Meng, F. Cheng, L. Zhou, Transient responses of functionally graded magneto-electro-elastic structures with holes in thermal environment using stabilized node-based smoothed radial point interpolation method, Int. J. Mech. Sci. 185 (2020) 105870, https://doi.org/10.1016/j.ijmecsci.2020.105870.

[48] S. Ren, G. Meng, B. Nie, L. Zhou, H. Zhao, A novel stabilized node-based smoothed radial point interpolation method (SNS-RPIM) for coupling analysis of magneto-electro-elastic structures in hygrothermal environment, Comput. Methods Appl. Mech. Eng. 365 (2020) 112975, https://doi.org/10.1016/j.cma.2020.112975.

[49] L. Zhou, M. Li, Y. Cai, H. Zhao, E. Zhao, The multi-physic cell-based smoothed finite element method for dynamic characterization of magneto-electro-elastic structures under thermal conditions, Compos. Struct. 240 (2020) 112045, https://doi.org/10.1016/j.compstruct.2020.112045.

[50] L. Zhou, X. Li, M. Li, K.K. Zur, The smoothed finite element method for time-dependent mechanical responses of MEE materials and structures around Curie temperature, Comput. Methods Appl. Mech. Eng. 370 (2020) 113241, https://doi.org/10.1016/j.cma.2020.113241.

[51] L. Zhou, B. Nie, C. Ren, S. Ren, G. Meng, Dynamic analysis of magneto-electro-elastic nanostructures using node-based smoothed radial point interpolation method combined with micromechanics-based asymptotic homogenization technique, J. Intell. Mater. Syst. Struct. 31 (2020), https://doi.org/10.1177/1045389X20935572.

[52] S. Ren, V. Mahesh, G. Meng, L. Zhou, Static responses of magneto-electro-elastic structures in moisture field using stabilized node-based smoothed radial point interpolation method, Compos. Struct. 252 (2020) 112696, https://doi.org/10.1016/j.compstruct.2020.112696.

[53] M. Li, M. Liu, L. Zhou, The static behaviors study of magneto-electro-elastic materials under hygrothermal environment with multi-physical cell-based smoothed finite element method, Compos. Sci. Technol. 193 (2020) 108130, https://doi.org/10.1016/j.compscitech.2020.108130.

[54] What is a neural net?, Available online: http://www.cormactech.com/neunet/whatis.html, 2019.

[55] A. Issa, PhD Thesis, in: A. Issa (Ed.), Computational Control of Laser Systems for Micro-machining, Dublin City University, 2007.

[56] J. Ye, X.C. Yuan, G. Zhou, Genetic algorithm for optimization design of diffractive optical elements in laser beam shaping, Proc. SPIE-Int. Soc. Opt. Eng. 4594 (2001) 118–127, https://doi.org/10.1117/12.446537.

[57] G.G. Wang, S.Q. Xie, Optimal process planning for a combined punch-and-laser cutting machine using ant colony, Int. J. Prod. Res. 43 (2005) 2195–2216, https://doi.org/10.1080/00207540500070376.

[58] H. Shen, Y.J. Shi, Z.Q. Yao, J. Hu, Fuzzy logic model for bending angle in laser forming, Mater. Sci. Technol. 22 (2006) 981–986, https://doi.org/10.1179/174328406X100725.

[59] A.M. Deus, J. Mazumder, Two-dimensional thermo-mechanical finite element model for laser cladding, Laser Materials Processing B174 (1996).

[60] M. Esmailzadeh, K.M. Aghaie, Finite element and artificial neural network analysis of ECAP, Comput. Mater. Sci. 63 (2012) 127–133, https://doi.org/10.1016/j.commatsci.2012.05.075.

[61] A. Miguel, R. Komal, D.T. Konstantinos, P.R. Tiago, Neural network-based formula for the buckling load prediction of I-section cellular steel beams, Computers 8 (2019) 1–26, https://doi.org/10.3390/computers8010002.

[62] J.N. Reddy, in: J.N. Reddy (Ed.), Theory and Analysis of Elastic Plates and Shells, second ed., CRC Press, 2006.